A New Synthesis and Design Approach of a Complex Termination Impedance Bandpass Filter

Phirun Kim, *Member, IEEE*, and Yongchae Jeong, *Senior Member, IEEE*

***Abstract*— A new synthesis for the design of a bandpass filter (BPF) with arbitrary real and/or complex termination impedances is presented in this paper. The proposed BPF can be terminated with arbitrary complex termination impedances simply by adding series transmission lines (TLs) to the first and the last coupled resonators. For design freedom, the characteristic impedances of the additional TLs can be chosen arbitrarily. Moreover, the proposed filter can be designed in either even- or odd-ordered stages using a λ/4 stepped impedance resonator (SIR). For the validation of the proposed filter, two- and three-stage λ/4 SIR BPFs with $Z_S = 30 + j10$ Ω, $Z_L = 50$ Ω, and $Z_S = 50$ Ω, $Z_L = 100 + j100$ Ω, respectively, were designed and fabricated at the center frequency (f_0) of 2.6 GHz. The measured results are consistent with the simulation results.**

***Index Terms*— Bandpass filter (BPF), complex impedance, coupled line, stepped-impedance resonator (SIR), T-type network.**

I. Introduction

THE bandpass filter (BPF) with real and/or complex termination impedances is an important circuit in most microwave applications for directly matching the adjacent circuits with a compact size, low-loss, and high-selective filtering response. A quarter-wavelength ($\lambda/4$) impedance transformer is suitable for real-to-real impedance transformation [1]. However, the out-of-band suppression of the $\lambda/4$ impedance transformer is poor. Recently, real-to-real impedance transformers with bandpass filtering response have been studied using parallel-coupled lines with shunt-coupled lines or transmission lines (TL) [2], [3], multisection parallel-coupled lines [4]–[6], stepped-impedance resonators (SIRs) [7], and pi-tapped feeds [8]. However, the unequal real-to-real termination impedance transformers with bandpass filtering response are not enough for the impedance matching networks of the power transistor, antenna, mixer, and RF harvesting system when real-to-complex impedance matching is required.

The matching networks have been presented and can be designed using lumped elements [9], TLs [10], stepped-impedance TL [11], coupled lines with open/short stub [12], and shunt-stub networks [13], [14]. The design formulas were previously considered only for center frequency (f_0), but the out-of-band suppression characteristics were poor. Recently, the evanescent-mode cavity and microstrip line matching networks with filtering response were designed for use in high-power and high-efficiency amplifiers [15]–[20]. In [15], a two-stage cavity resonator BPF with complex termination was studied under a coupling matrix. The complex termination impedance could be obtained by modifying the coupling matrix of the 50-Ω termination BPF. In [16]–[18], the microstrip line matching networks were designed by converting ladder *LC* lumped elements in the low-pass filter (LPF) of [22] to the distributed elements. These networks provided good passband characteristics; however, the lower and higher stopband attenuations were limited. The LPFs based on arbitrary real-to-real termination impedance were designed, after which the real-to-complex termination could be obtained by adjusting the reactance element values at the complex impedance terminal. In [19] and [20], the impedance transformers with bandpass filtering response were used to design a high-efficiency and high-power amplifier. Similarly, the complex termination impedance of the transformer was obtained by optimizing that from the real-to-real termination impedance transformer. In [21], a new dual-band filter with complex termination impedances was proposed using a coupled resonator. However, there are no fabrication and measurement results.

The microstrip BPFs have generally been studied using equal termination impedances (i.e., 50 Ω) with a compact size, high selectivity, and controllable spurious performance [23]–[28]. However, the general microstrip BPF with complex termination impedance has not been widely studied to date. In [23], a $\lambda/4$ uniform impedance resonator with alternative J-/K-inverters was analyzed for the even-order Chebyshev BPF with equal termination impedances. Similarly, in [24] and [25], the BPFs with controllable spurious performance were designed using $\lambda/4$ SIRs. However, it is observed that these BPFs can be designed only with the even-order stages.

In this paper, a new design methodology for microstrip BPFs with arbitrary real and/or complex terminations impedance is investigated mathematically using narrowband $\lambda/4$ SIRs. The proposed filter can provide controllable spurious characteristics with either even- or odd-order stages. The K-inverter and its T-type equivalent circuit are derived

Manuscript received July 27, 2018; revised November 26, 2018 and January 15, 2019; accepted March 21, 2019. Date of publication April 23, 2019; date of current version June 4, 2019. This research was supported by the Research Base Construction Fund Support Program funded by Chonbuk National University in 2018. *(Corresponding author: Yongchae Jeong.)*

The authors are with the Division of Electronics and Information Engineering, IT Convergence Research Center, Chonbuk National University, Jeonju 54896, South Korea (e-mail: ycjeong@jbnu.ac.kr).

Color versions of one or more of the figures in this paper are available online at http://ieeexplore.ieee.org.

Digital Object Identifier 10.1109/TMTT.2019.2910110

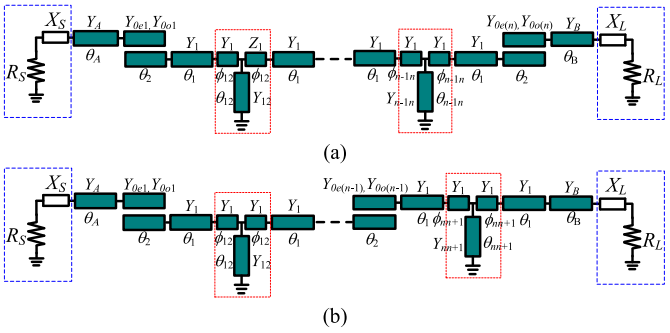

Fig. 1. Proposed structures of complex termination impedances $\lambda/4$ SIR BPF. (a) Even-order stage. (b) Odd-order stage.

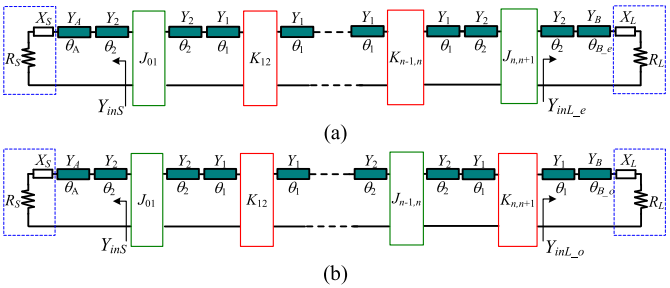

Fig. 2. Equivalent circuit of proposed complex termination impedances $\lambda/4$ SIR BPF. (a) Even-order stage. (b) Odd-order stage.

through a straightforward technique. The design formulas have been mathematically checked and verified by lossless circuit simulations, electromagnetic (EM) simulations, and measurements. Moreover, the proposed BPF can be simultaneously designed with a predefined fractional bandwidth (FBW), number of stages, passband response (Chebyshev or Butterworth), and complex termination impedances.

II. Circuit Analysis

Fig. 1 shows the proposed structures of complex termination impedances $\lambda/4$ SIR BPF in even-and odd-order stages, respectively, where the complex termination impedances are $Z_S = R_S \pm jX_S$ and $Z_L = R_L \pm jX_L$. The filter can be designed for real-to-real, real-to-complex, or complex-to-complex termination impedances as desired. The proposed structure consists of open-ended parallel coupled TLs and T-type TLs cascaded alternatively. For the even-order, the network is ended with the parallel-coupled line and series TL with a characteristic impedance of Y_B $(=1/Z_B)$, as seen in Fig. 1(a). For the odd-order, the network is ended with the T-type TLs and series TL with a characteristic impedance of Z_B, as seen in Fig. 1(b). The electrical lengths of resonator and series TLs of T-network can be added to or subtracted from adjacent TLs with the same characteristic impedances. The equivalent circuits of Fig. 1 can be modeled with alternative J- and K-inverters as shown in Fig. 2 for even- and odd-order stages, respectively, where Y_2 $(=1/Z_2)$ is the image admittance of parallel-coupled lines [6], [7]. Y_2 and θ_2 can be varied according to the stepped-impedance ratio $(R_Z = Y_1/Y_2)$ [29], where Y_A $(=1/Z_A)$ and Y_B are arbitrarily chosen variables. In case of conventional $\lambda/4$ SIR BPFs [24], the characteristic impedance of Z_2 is always equal to the termination impedance, i.e., $Z_2 = Z_0 = 50\ \Omega$, because θ_2 is less than $\pi/2$ at the center frequency (f_0). In the conditions of $\theta_2 < \pi/2$ and $Z_2 \neq Z_0$, the input admittances (Y_{inS} and Y_{inL}) of the conventional $\lambda/4$ SIR BPF will be complex admittances. However, these complex admittances cannot directly match the adjacent J- or K-inverters. For a solution to the complex admittance, the TLs with electrical parameters of Z_A with θ_A and Z_B with θ_B are added to the input and output ports of the conventional $\lambda/4$ SIR BPF. The addition of series TL sections is more beneficial than the addition of shunt TLs for capacitive or inductive effects in terms of bandwidth and simplicity. By adding the TLs, Z_2 of resonators can choose arbitrary impedances when the termination impedances (Z_S and Z_L) are arbitrary real and/or complex values.

A. Even-Order Bandpass Filter

Fig. 2(a) shows the equivalent circuit of the proposed complex termination impedances $\lambda/4$ SIR BPF with even-order stages. The resonators are coupled with J-/K-inverters alternatively, where the J- and K-inverters are implemented with parallel-coupled line and T-type network, respectively. Since the last inverter ends with a J-inverter, the input and output network syntheses are the same. The T-type network consists of two series TLs with a short-circuited shunt stub, and designed equations will be discussed in the next section. Since J-/K-inverters cannot directly match the complex termination, the complex impedance must be transformed to real impedance. From Fig. 2(a), the input admittance of Y_{inS} can be derived as follows:

$$Y_{inS} = \mathrm{Re}(Y_{inS}) + j\,\mathrm{Im}(Y_{inS}) \tag{1}$$

where

$$\mathrm{Re}(Y_{inS}) = Y_2 \frac{\left[\begin{array}{l}(Y_2A_3 - A_2\tan\theta_2)(A_1 - Y_2A_4\tan\theta_2)\\ +(A_2 + Y_2A_3\tan\theta_2)(Y_2A_4 + A_1\tan\theta_2)\end{array}\right]}{(Y_2A_3 - A_2\tan\theta_2)^2 + (Y_2A_4 + A_1\tan\theta_2)^2} \tag{2a}$$

$$\mathrm{Im}(Y_{inS}) = Y_2 \frac{\left[\begin{array}{l}(A_2 + Y_2A_3\tan\theta_2)(Y_2A_3 - A_2\tan\theta_2)\\ -(A_1 - Y_2A_4\tan\theta_2)(Y_2A_4 + A_1\tan\theta_2)\end{array}\right]}{(Y_2A_3 - A_2\tan\theta_2)^2 + (Y_2A_4 + A_1\tan\theta_2)^2} \tag{2b}$$

$$A_1 = Y_A - Y_A^2 X_S \tan\theta_A \tag{2c}$$

$$A_2 = Y_A^2 R_S \tan\theta_A \tag{2d}$$

$$A_3 = R_S Y_A \tag{2e}$$

$$A_4 = X_S Y_A + \tan\theta_A. \tag{2f}$$

R_S and X_S are the real and imaginary parts of source impedance, respectively.

The electrical length of resonators with characteristic admittance of Y_2 can be calculated using R_Z and $Y_1(=1/Z_1)$. Therefore, the TLs with electrical parameters of Y_A with θ_A and Y_B with θ_{B_e} are used to adjust the input admittances of Y_{inS} and Y_{inL_e} for pure real admittances. For this, the electrical length of θ_A is derived as follows by substituting (2b) equal to 0:

$$\theta_A = \tan^{-1}\left(\frac{-C_2 \pm \sqrt{C_2^2 - 4C_1C_3}}{2C_1}\right) \tag{3}$$

where

$$C_1 = \left[Y_A^2 X_S B_1 - Y_A^4\left(R_S^2 + X_S^2\right)\tan\theta_2 + B_2\right] \tag{4a}$$

$$C_2 = \left\{\left[Y_A^2(R_S^2 + X_S^2) - 1\right]B_1 + 2X_S\left(Y_A^2\tan\theta_2 + B_2\right)\right\}Y_A \tag{4b}$$

$$C_3 = Y_A^2\left[B_2\left(R_S^2 + X_S^2\right) - X_S B_1 - \tan\theta_2\right] \tag{4c}$$

$$B_1 = (1 - \tan^2\theta_2)Y_2 \tag{4d}$$

$$B_2 = Y_2^2\tan\theta_2 \tag{4e}$$

and θ_A must be a positive real number for given Z_A and other variable values. In practical, Z_A can be chosen within the realizable range of 20–130 Ω.

Similarly, the input admittance of Y_{inL_e} can be derived as follows:

$$Y_{inL\_e} = \mathrm{Re}(Y_{inL\_e}) + j\mathrm{Im}(Y_{inL\_e}) \tag{5}$$

where

$$\mathrm{Re}(Y_{inL\_e}) = Y_2\frac{\left[\begin{array}{l}(Y_2A_7 - A_6\tan\theta_2)(A_5 - Y_2A_8\tan\theta_2)\\ +(A_6 + Y_2A_7\tan\theta_2)(Y_2A_8 + A_5\tan\theta_2)\end{array}\right]}{(Y_2A_7 - A_6\tan\theta_2)^2 + (Y_2A_8 + A_5\tan\theta_2)^2} \tag{6a}$$

$$\mathrm{Im}(Y_{inL\_e}) = Y_2\frac{\left[\begin{array}{l}(A_6 + Y_2A_7\tan\theta_2)(Y_2A_7 - A_6\tan\theta_2)\\ -(A_5 - Y_2A_8\tan\theta_2)(Y_2A_8 + A_5\tan\theta_2)\end{array}\right]}{(Y_2A_7 - A_6\tan\theta_2)^2 + (Y_2A_8 + A_5\tan\theta_2)^2} \tag{6b}$$

$$A_5 = Y_B - Y_B^2 X_L\tan\theta_{B\_e} \tag{6c}$$

$$A_6 = Y_B^2 R_L\tan\theta_{B\_e} \tag{6d}$$

$$A_7 = R_L Y_B \tag{6e}$$

$$A_8 = X_L Y_B + \tan\theta_{B\_e}. \tag{6f}$$

In order to obtain a real value of Y_{inL_e}, (6b) must be equal to 0. Thus, the electrical length of θ_{B_e} can be derived as follows:

$$\theta_{B\_e} = \tan^{-1}\left(\frac{-C_5 \pm \sqrt{C_5^2 - 4C_4C_6}}{2C_4}\right) \tag{7}$$

where

$$C_4 = \left[Y_B^2 X_L B_1 - Y_B^4\left(R_L^2 + X_L^2\right)\tan\theta_2 + B_2\right] \tag{8a}$$

$$C_5 = \left\{\left[Y_B^2(R_L^2 + X_L^2) - 1\right]B_1 + 2X_L\left(Y_B^2\tan\theta_2 + B_2\right)\right\}Y_B \tag{8b}$$

$$C_6 = Y_B^2\left[B_2\left(R_L^2 + X_L^2\right) - X_L B_1 - \tan\theta_2\right]. \tag{8c}$$

Since Z_A must have a feasible range with microstrip technology, Z_A is chosen within the practical range of 20–130 Ω. However, it is very difficult to define realizable source/load impedance ranges for fabrication difficulty. In order to solve this problem, the relations between θ_A and Z_A are calculated with different real and complex termination impedances and plotted in Fig. 3. From (3), there are two possible results for given Z_A and other variables values. The electrical length of θ_A is essentially varied with the termination impedance and can be adjusted by changing Z_A.

Fig. 3 depicts two different curves, one for the negative reactances ($-X_S$) and another for the positive reactances ($+X_S$) by fixing $R_S = 5$ Ω. For negative values of X_S, the length of θ_A has two possible design curves for $X_S = -40$ to -140 Ω; however, θ_A has only one design curve for $X_S = -5$ and -300 Ω. For positive values of X_S, θ_A has two possible design curves when $X_S = +40$ to $+70$ Ω, whereas θ_A has one design curve for $X_S = +5$ Ω and $+100$ to $+300$ Ω. In the case of dual results, both values can be used to design the filter, but the shorter θ_A is preferable for compact circuit size. However, if the shorter θ_A causes fabrication difficulty of Z_A, the longer θ_A is preferable. The calculations for Fig. 3 were done by fixing $Z_1 = 130$ Ω, $Z_2 = 50$ Ω, and $R_S = 5$ Ω.

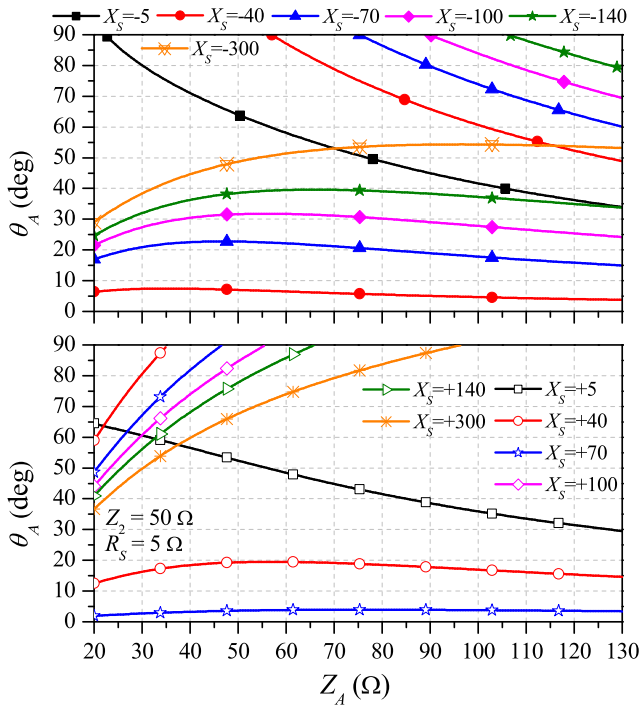

Fig. 3. Electrical lengths of θ_A according to the characteristic impedances Z_A and reactance X_S in conditions of $Z_1 = 130$ Ω, $Z_2 = 50$ Ω, and $R_S = 5$ Ω.

Similarly, Fig. 4 depicts different curves, one is for fixing $X_S = -10$ Ω and another is for $X_S = +10$ Ω whereas R_S varies from 5 to 500 Ω. In the case of $X_S = -10$ Ω, θ_A has two design curves for $R_S = 50$ Ω. θ_A is required 60.2° for all R_S from 5 to 500 Ω when $Z_A = 62$ Ω. Moreover, θ_A has two designed curves for $R_S = 50$ Ω when $X_S = +10$ Ω. θ_A is required 50° for all R_S from 5 to 500 Ω when $Z_A = 37$ Ω. The calculations for Fig. 4 were done by fixing $Z_1 = 130$ Ω and $Z_2 = 50$ Ω.

B. Odd-Order Bandpass Filter

Fig. 2(b) shows the equivalent circuit of the proposed complex termination impedances $\lambda/4$ SIR BPF with odd-order stages. The source termination structure is the same as that of the even-order filter; however, the final order structure is terminated with a T-type network and series TL with characteristic admittance of Y_B. In this case, the input admittance (Y_{inL_o}) looking into the load is derived as follows:

$$Y_{inL\_o} = \mathrm{Re}(Y_{inL\_o}) + j\mathrm{Im}(Y_{inL\_o}) \tag{9}$$

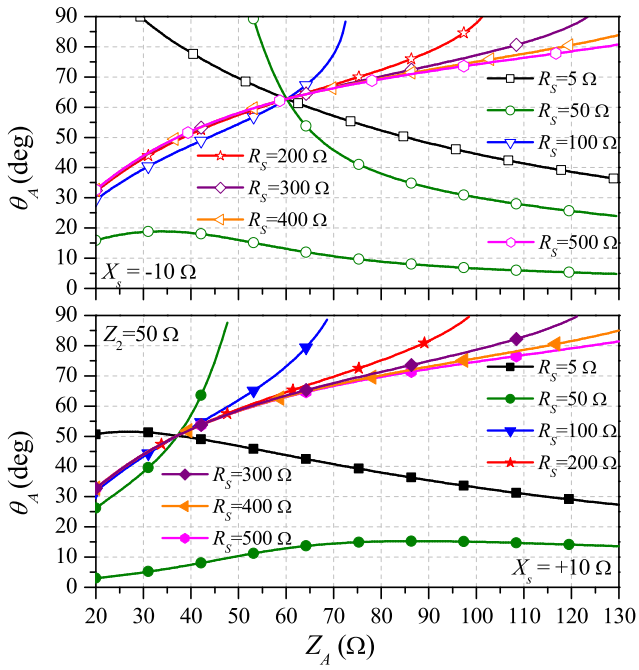

Fig. 4. Electrical lengths of θ_A according to the characteristic impedances Z_A and resistors R_S in conditions of $Z_1 = 130\ \Omega$, $Z_2 = 50\ \Omega$, and $X_S = \pm 10\ \Omega$.

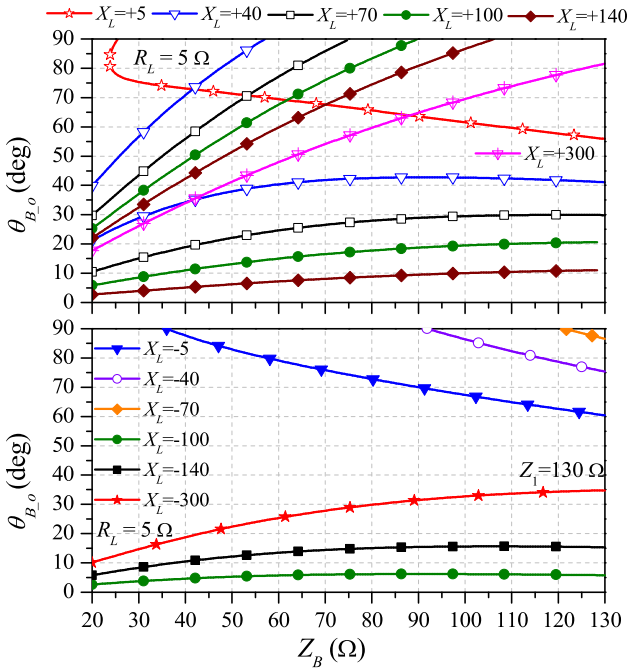

Fig. 5. Electrical lengths of θ_{B_o} according to the characteristic impedances Z_B and reactance X_L in conditions of $Z_1 = 130\ \Omega$, $Z_2 = 50\ \Omega$, and $R_L = 5\ \Omega$.

where

$$\mathrm{Re}(Y_{inL\_o}) = Y_1 \frac{\begin{bmatrix}(Y_1A_{11} - A_{10}\tan\theta_1)(A_9 - Y_1A_{12}\tan\theta_1)\\ +(A_{10} + Y_1A_{11}\tan\theta_1)(Y_1A_{12} + A_9\tan\theta_1)\end{bmatrix}}{(Y_1A_{11} - A_{10}\tan\theta_1)^2 + (Y_1A_{12} + A_9\tan\theta_1)^2} \tag{10a}$$

$$\mathrm{Im}(Y_{inL\_o}) = Y_1 \frac{\begin{bmatrix}(A_{10} + Y_1A_{11}\tan\theta_1)(Y_1A_{11} - A_{10}\tan\theta_1)\\ -(A_9 - Y_1A_{12}\tan\theta_1)(Y_1A_{12} + A_9\tan\theta_1)\end{bmatrix}}{(Y_1A_{11} - A_{10}\tan\theta_1)^2 + (Y_1A_{12} + A_9\tan\theta_1)^2} \tag{10b}$$

$$A_9 = Y_B - Y_B^2 X_L \tan\theta_{B\_o} \tag{10c}$$

$$A_{10} = Y_B^2 R_L \tan\theta_{B\_o} \tag{10d}$$

$$A_{11} = R_L Y_B \tag{10e}$$

$$A_{12} = X_L Y_B + \tan\theta_{B\_o}. \tag{10f}$$

Similar to the even order, Y_{inL-o} must be pure real admittance. Thus, the electrical length of θ_{B_o} can be derived as follows by substituting (10b) equal to 0:

$$\theta_{B\_o} = \tan^{-1}\left(\frac{-C_8 \pm \sqrt{C_8^2 - 4C_7C_9}}{2C_7}\right) \tag{11}$$

where

$$C_7 = \left[Y_B^2 X_L B_3 - Y_B^4\left(R_L^2 + X_L^2\right)\tan\theta_1 + B_4\right] \tag{12a}$$

$$C_8 = \left\{\left[Y_B^2(R_L^2 + X_L^2) - 1\right]B_3 + 2X_L\left(Y_B^2\tan\theta_1 + B_4\right)\right\}Y_B \tag{12b}$$

$$C_9 = Y_B^2\left[B_4\left(R_L^2 + X_L^2\right) - X_L B_3 - \tan\theta_1\right] \tag{12c}$$

$$B_3 = (1 - \tan^2\theta_1)Y_1 \tag{12d}$$

$$B_4 = Y_1^2\tan\theta_1. \tag{12e}$$

From (3), (7), and (11), the input admittances of Y_{inS} and Y_{inL} remain as pure real admittance for given Y_A, Y_B, and other variables. The relations between θ_{B_o} and Z_B are studied and plotted in Fig. 5 with different values of X_L. θ_{B_o} can be adjusted by changing Z_B. Fig. 5 depicts two different curves, one is for positive values of X_L and the another is for negative values of X_L by fixing $Z_1 = 130\ \Omega$, $Z_2 = 50\ \Omega$, and $R_L = 5\ \Omega$. θ_{B_o} has two curves for $X_L = +40$ to $+140\ \Omega$; however, θ_{B_o} has one curve for $X_L = +5\ \Omega$ and $X_L = +300\ \Omega$. For negative values of X_L, θ_{B_o} has one design curve for all $X_L = -5$ to $-300\ \Omega$.

Fig. 6 depicts different curves for fixing $X_L = -10\ \Omega$ and $X_L = +10\ \Omega$, where R_L varies from 5 to 500 Ω. In the case of $X_L = -10\ \Omega$, θ_{B_o} has one curve for all R_S, varying from 5 to 500 Ω. Similarly, θ_{B_o} and Z_B are required to be 58° and 118 Ω, respectively, for varying R_S from 5 to 500 Ω and for $X_L = +10\ \Omega$. The calculations for Fig. 6 were done by fixing $Z_1 = 130\ \Omega$ and $Z_2 = 50\ \Omega$.

C. Stepped-Impedance Resonator and J-/K-inverters

Fig. 7 shows a $\lambda/4$ SIR structure with open- and short-ends. From [29], the resonance condition can be obtained as follows for $\theta_1 = \theta_2 = \theta_0$:

$$\tan^2\theta_0 = R_Z = \frac{Z_2}{Z_1} = \frac{Y_1}{Y_2}. \tag{13}$$

In this paper, the characteristic impedances of Z_1 and Z_2 can be arbitrarily chosen. The relationship among R_Z, normalized spurious frequencies, and Z_1 is shown in Fig. 8. Herein, the spurious frequencies are moved far away from the fundamental frequency as R_Z decreases and Z_1 increases. Moreover, the slope parameters of resonators are derived as $b = \theta_0 Y_2$ and $x = \theta_0 Z_1$.

Based on the previous section, the source and load input admittances are checked as pure real admittances.

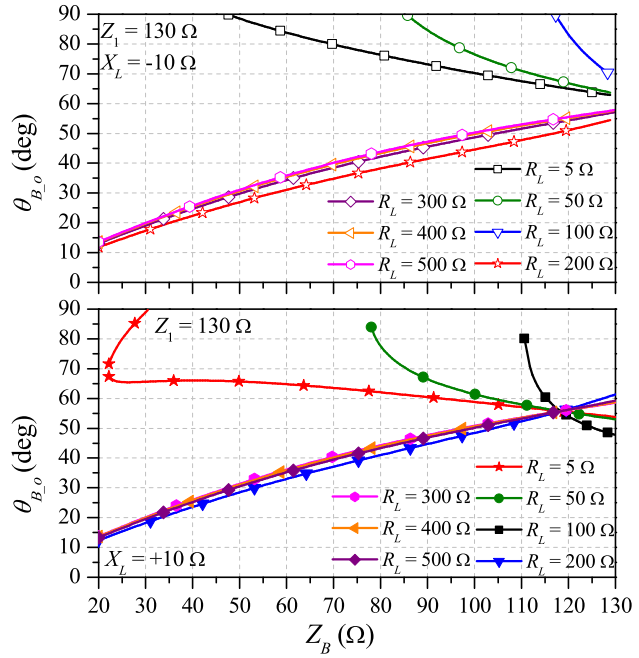

Fig. 6. Electrical lengths of θ_{B_o} according to the characteristic impedances Z_B and resistors R_L in conditions of $Z_1 = 130\ \Omega$, $Z_2 = 50\ \Omega$, and $X_L = \pm 10\ \Omega$.

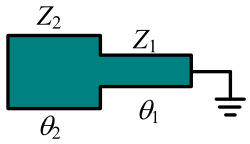

Fig. 7. Electrical parameters of SIR.

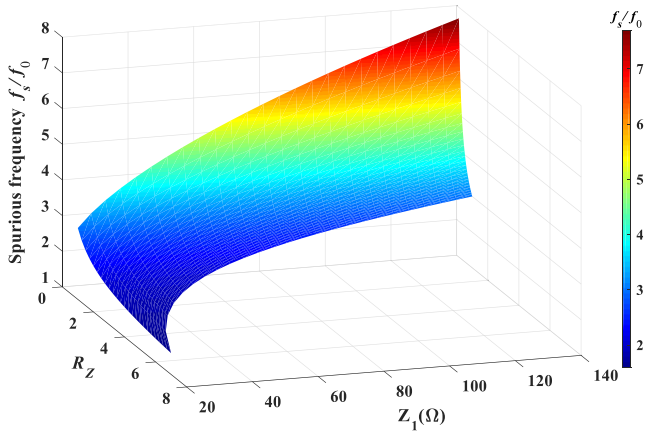

Fig. 8. Spurious frequency of SIR according to Z_1 and R_Z.

Then, the impedance and the admittance inverters (K- and J-inverters) of the even- and odd-order $\lambda/4$ SIR BPFs can be calculated as follows:

$$J_{01} = \sqrt{\frac{\mathrm{Re}(Y_{ins})\mathrm{FBW}\theta_0}{Z_2 g_0 g_1}} \tag{14a}$$

$$K_{j,j+1} = \frac{Z_1\theta_0\mathrm{FBW}}{\sqrt{g_j g_{j+1}}}, \quad @j : 1, 3, 5, \ldots \tag{14b}$$

$$J_{i,i+1} = \frac{\mathrm{FBW}\theta_0}{Z_2\sqrt{g_i g_{i+1}}}, \quad @i : 2, 4, 6, \ldots \tag{14c}$$

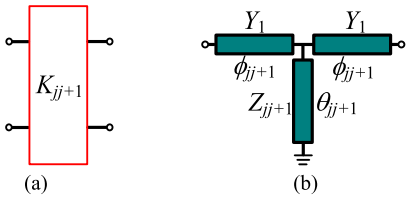

Fig. 9. Two-port inverter. (a) K-inverter. (b) Its T-type equivalent circuit.

$$K_{p,p+1} = \sqrt{\frac{\mathrm{Re}(Z_{inL\_o})\mathrm{FBW}\theta_0 Z_1}{g_p g_{p+1}}}, \quad @p : \text{odd number} \tag{14d}$$

$$J_{m,m+1} = \sqrt{\frac{\mathrm{Re}(Y_{inL\_e})\mathrm{FBW}\theta_0}{Z_2 g_m g_{m+1}}}, \quad @m : \text{even number} \tag{14e}$$

where g_0, g_1, g_i, g_j, g_p, and g_m are the elements of the low-pass prototype. FBW is the fractional bandwidth of the passband. $\mathrm{Re}(Y_{inS})$ is a real term of Y_{inS} and can be obtained from (2a). $\mathrm{Re}(Y_{inL\_o})$ and $\mathrm{Re}(Y_{inL\_e})$ are the real terms of Y_{inL_o} and Y_{inL_e} and can be found from (6a) and (10a), respectively.

D. Implementations of J- and K-inverters

The parallel-coupled lines with open-circuit stubs can be modeled as J-inverters and widely used in the designs of coupled BPF [29]. The even- and odd-mode admittances of coupled lines with arbitrary electrical lengths can be derived as follows:

$$(Z_{0e})_{i+1} = Z_2\frac{1 + J_{i,i+1}Z_2\csc\theta + J_{i,i+1}^2 Z_2^2}{1 - J_{i,i+1}^2 Z_2^2\cot^2\theta} \tag{15a}$$

$$(Z_{0o})_{i+1} = Z_2\frac{1 - J_{i,i+1}Z_2\csc\theta + J_{i,i+1}^2 Z_2^2}{1 - J_{i,i+1}^2 Z_2^2\cot^2\theta} \tag{15b}$$

where Z_2 is an image impedance of the coupled line and can be chosen as an arbitrary impedance. i is the even number starting from 0.

Fig. 9 shows the K-inverter and its T-type equivalent circuit. The equivalent circuit consists of two TLs with electrical parameters of Y_1 and ϕ_{jj+1}, and a shunt short-circuit stub TL with electrical parameters of $Y_{jj+1}(=1/Z_{jj+1})$ and θ_{jj+1}. The design equations can be obtained by equating the ABCD parameters of the K-inverter and its T-type equivalent circuit. Accordingly, the electrical lengths of θ_{jj+1} and ϕ_{jj+1} are derived as follows:

$$\theta_{jj+1} = \tan^{-1}\frac{Y_{jj+1}Z_1\cos\phi_{jj+1}\sin\phi_{jj+1}}{\sin^2\phi_{jj+1} - \cos^2\phi_{jj+1}}, \quad j : 1, 3, 5 \ldots, p \tag{16}$$

where

$$\phi_{jj+1} = -\tan^{-1}\frac{K_{jj+1}}{Z_1}. \tag{17}$$

K_{jj+1} is a K-inverter value and can be obtained from (14). The characteristic impedance of Z_1 is already equal to the adjacent lines of the same impedance of resonators. Based on (17), since Z_1 is always greater than 1, ϕ_{jj+1} is always

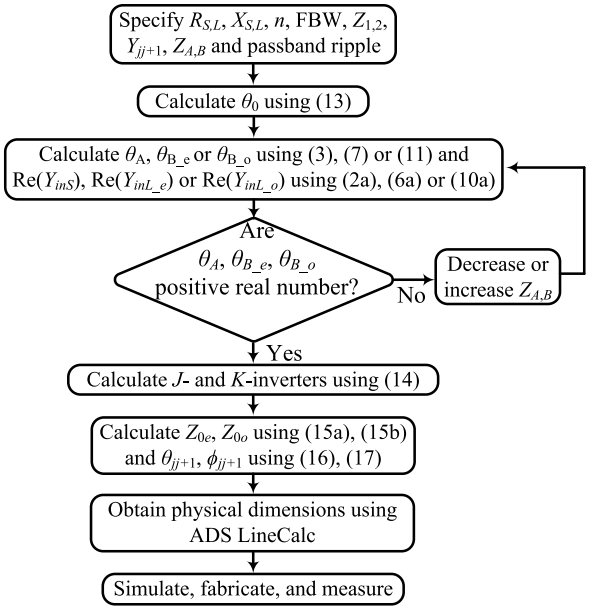

Fig. 10. Calculation flowchart for circuit parameters of proposed complex terminations BPF.

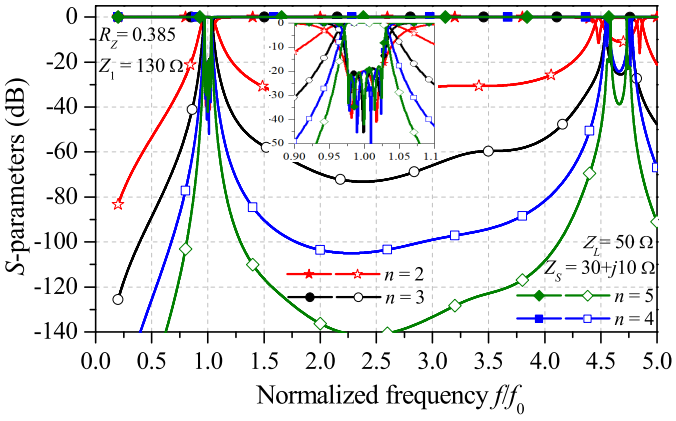

Fig. 11. S-parameters of Chebyshev response with different n.

negative and can be subtracted from the adjacent lines of the same impedance TLs. Thus, the length of the resonator with characteristic impedance Z_1 will be slightly shortened. The filter performance is not influenced although the resonator length is slightly shortened. The electrical length of θ_{jj+1} can be calculated by choosing Z_{jj+1} arbitrarily.

Fig. 10 summarizes the design flowchart of calculation for circuit parameters of the proposed complex termination impedance $\lambda/4$ SIR BPF.

E. Design Examples

In order to demonstrate the previous analysis, $\lambda/4$ SIR BPFs with complex termination impedances and arbitrary Z_2 are designed and simulated using lossless TLs and coupled lines of the advance design system (ADS) tool. Fig. 11 shows the frequency response of the proposed BPF with different n. In this simulation, the termination impedances of Z_S and Z_L are fixed with a complex impedance of $(30+j10)$ Ω and a real impedance of 50 Ω, respectively, and Chebyshev polynomial

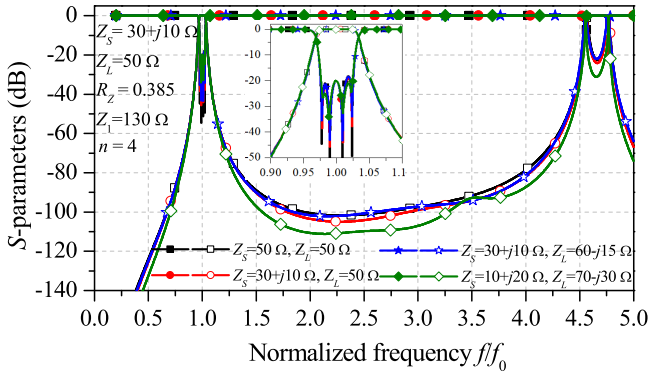

Fig. 12. S-parameters of Chebyshev response with different termination impedances.

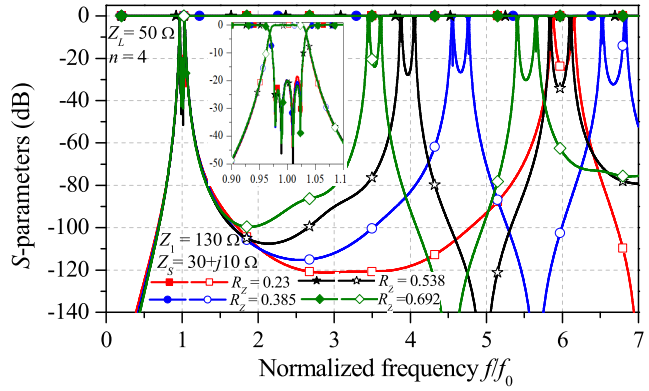

Fig. 13. S-parameters of Chebyshev response with different R_Z.

prototype element values are used. As shown in Fig. 11, the stopband attenuation is highly increased as n increases. The spurious frequency is located at $4.6f_0$ with $R_Z = 0.385$. Moreover, the FBWs of the passband are nearly identical for all n. From these simulations, it has been proven that the proposed BPF can be designed with even- and odd-order stages.

Fig. 12 shows frequency responses of the proposed BPF with different termination impedances. The passband responses are identical for all termination impedances. However, the stopband attenuation is slightly improved for $Z_S = 10 + j20\ \Omega$ and $Z_L = 70 - j30\ \Omega$. Similarly, the first spurious is located at $4.6f_0$ with $R_Z = 0.385$. From these simulations, it has been proven that the proposed BPF can be designed with real-to-real, real-to-complex, and complex-to-complex termination impedances.

Fig. 13 shows the frequency responses of the proposed BPF with different R_Z. In this simulation, the termination impedances are fixed at $Z_S = 30 + j10\ \Omega$ and $Z_L = 50\ \Omega$. The Z_1 is fixed to be 130 Ω and Z_2 is varied from 30 to 90 Ω. As shown in Fig. 13, the spurious frequencies are moved far away from f_0 as R_Z decreases. Moreover, the FBW is maintained at about 5% for all Z_2. Thus, it can be observed herein that the proposed BPF can be designed for arbitrary Z_2 and complex termination impedances with the controllable spurious characteristic. The calculations and specifications of all variables of Figs. 11–13 are listed in Table I.

TABLE I

CALCULATED VARIABLES OF THE PROPOSED BPF WITH DIFFERENT n, TERMINATION IMPEDANCE, AND Z_2

ripple = 0.043 dB, FBW = 5 %, Z_1 = 130 Ω, Z_2 = 50 Ω Z_A = 40 Ω, Z_{12} = Z_{34} = Z_{56} = 80 Ω, Z_S = 30+j10 Ω, Z_L = 50 Ω						Order n
Z_{0e1}/Z_{0o1}	ϕ_{12}/θ_{12}	Z_{0e2}/Z_{0o2}	ϕ_{34}/θ_{34}	Z_{0e3}/Z_{0o3}	ϕ_{56}/θ_{56}	$\theta_A/\theta_B/Z_B$	
74.98 /37.73	-2.63/4.29	82.35 /36.32				46.805 /26.26/45	2
71.01 /38.73	-1.64/2.66	52.87 /47.43	-11.95/19.8			46.805 /76.04/90	3
69.77 /39.08	-1.45/2.35	51.91 /48.22	-1.45/2.35	75.15 /37.69		46.805 /26.26/45	4
69.22 /39.25	-1.37/2.23	51.73 /48.38	-1.01/1.64	52.38 /47.82	-11.2/18.53	46.805 /76.04/90	5
ripple = 0.043 dB, FBW = 5 %, Z_A = 40 Ω, Z_B = 45 Ω, Z_{12} = Z_{34} = 80 Ω, Z_1 = 130 Ω, Z_2 = 50 Ω, n = 4						Term. Impe. Z_S/Z_L [Ω]	
Z_{0e1}/Z_{0o1}	ϕ_{12}/θ_{12}	Z_{0e2}/Z_{0o2}	ϕ_{34}/θ_{34}	Z_{0e3}/Z_{0o3}	θ_A/θ_B		
77.103 /37.27	-1.45/2.35	51.91 /48.22	-1.45/2.35	75.15 /37.69	25.83 /26.26	50/50	
69.77 /39.08	-1.45/2.35	51.91 /48.22	-1.45/2.35	75.15 /37.69	46.805 /26.26	30+j10/50	
69.77 /39.08	-1.45/2.35	51.91 /48.22	-1.45/2.35	82.63 /36.28	46.805 /32.61	30+j10/60-j15	
59.08 /43.35	-1.45/2.35	51.91 /48.22	-1.45/2.35	91.01 /35.19	36.34 /35.09	10+j20/70-j30	
ripple = 0.043 dB, FBW = 5 %, n = 4, Z_A = 60 Ω, Z_{12} = Z_{34} = 80 Ω, Z_S = 30+j10 Ω, Z_L = 50 Ω						Impedance Ratio Z_2/Z_1	
Z_{0e1}/Z_{0o1}	ϕ_{12}/θ_{12}	Z_{0e2}/Z_{0o2}	ϕ_{34}/θ_{34}	Z_{0e3}/Z_{0o3}	$\theta_A/\theta_B/Z_B$		
39.1 /24.36	-1.17/1.9	31.13 /28.95	-1.17/1.9	46.95 /22.16	21.8 /85.53/38	30/130	
63.96 /41.09	-1.45/2.35	51.91 /48.22	-1.45/2.35	69.27 /39.23	38.07 /25.14/70	50/130	
89.75 /57.46	-1.65/2.68	72.72 /67.47	-1.65/2.68	94.36 /55.79	48.03 /53.73/70	70/130	
116.55 /73.445	-1.81/2.94	93.55 /86.71	-1.81/2.94	123.09 /71.199	56.21 /74.25/70	90/130	

III. SIMULATION AND MEASUREMENT RESULTS

In order to experimentally validate the analysis, the microstrip line BPFs with complex termination impedances are designed and implemented on RT/Duriod 5880 substrate with $\varepsilon_r = 2.2$ and $h = 0.787$ mm. Two filters are designed at f_0 of 2.6 GHz with different specifications. The EM simulation is performed using HFSS v17.1 of Ansoft.

The measurements of the proposed BPF are summarized as follows.

1) The TRL calibration is performed by offsetting the lengths of the subminiature version A connectors at the reference impedance lines of two ports, as shown in Figs. 14 and 16.
2) The unequal termination impedances 2-port S-parameters are measured and extracted as an S2P file from the network analyzer.
3) Renormalizing the termination impedance with respect to the port impedances, i.e., 30 + j10 and 50 Ω, then the S-parameters with port impedances of 30 + j10 Ω and 50 Ω can be calculated using the ADS tool.

A. Two-Stage SIR BPF

The first BPF is designed for Chebyshev response with ripple of 0.043 dB, $R_S = 30 + j10$ Ω, $R_L = 50$ Ω, $Z_A = Z_B = 100$ Ω, $Z_1 = 110$ Ω, and $Z_2 = 80$ Ω ($R_Z = 0.73$). The calculated variables are $\theta_A = 35.67°$, $Z_{0e1} = 98.78$ Ω, $Z_{0o1} = 67.28$ Ω, $\phi_{12} = -3.35°$, $\theta_{12} = 4.62°$, $Z_{0e2} = 106.15$ Ω, $Z_{0o2} = 64.36$ Ω, and $\theta_B = 38.84°$. Fig. 14 shows the layout and a photograph of the fabricated filter. The physical dimensions from the EM simulation are shown in Table II.

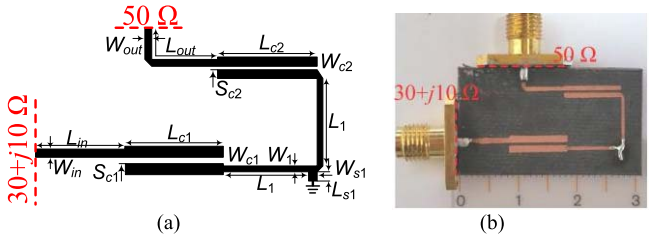

Fig. 14. Two-stage SIR BPF with the complex termination impedance. (a) Layout. (b) Photograph of fabricated circuit.

TABLE II

PHYSICAL DIMENSIONS OF THE TWO-STAGE SIR BPF WITH COMPLEX TERMINATION IMPEDANCE

W_{in} = 0.65	L_{c1} = 9.75	L_1 = 8.3	W_{c2} = 0.8	W_{out} = 0.65
L_{in} = 8.5	S_{c1} = 0.57	L_{S1} = 0.73	L_{c2} = 9.7	L_{out} = 9.43
W_{c1} = 1.05	W_1 = 0.54	W_{S1} = 0.85	S_{c2} = 0.4	

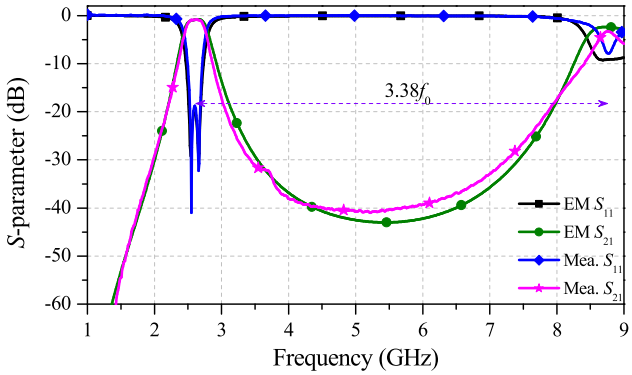

Fig. 15. Simulated and measured S-parameters of the two-stage SIR BPF with the complex impedance.

The overall circuit size is 28 mm × 14.42 mm. The EM simulation and measured S-parameters responses are shown in Fig. 15. The measured insertion and return losses are 0.89 and 19.33 dB at $f_0 = 2.6$ GHz, respectively. Moreover, the passband insertion and return losses are better than 1.1 and 18.8 dB from 2.53 to 2.67 GHz (FBW = 5.3%), respectively. The lower- and upper-side stopband rejections of 25 dB are obtained from dc to 2.09 GHz and 3.22 to 7.6 GHz, respectively. The spurious frequency occurs at 8.79 GHz (3.38f_0).

B. Three-Stage SIR BPF

The second BPF is designed for Chebyshev response with $n = 3$, $R_S = 50$ Ω, $R_L = 100 - j100$ Ω, $Z_A = 90$ Ω, $Z_B = 60$ Ω, $Z_1 = 130$ Ω, $Z_2 = 70$ Ω ($R_Z = 0.538$), $Z_{12} = 105$ Ω, and $Z_{34} = 70$ Ω. The calculated variables are $\theta_A = 40.24°$, $Z_{0e1} = 91.69$ Ω, $Z_{0o1} = 56.71$ Ω, $\phi_{12} = -1.87°$, $\theta_{12} = 2.31°$, $Z_{0e2} = 74.08$ Ω, $Z_{0o2} = 66.34$ Ω,

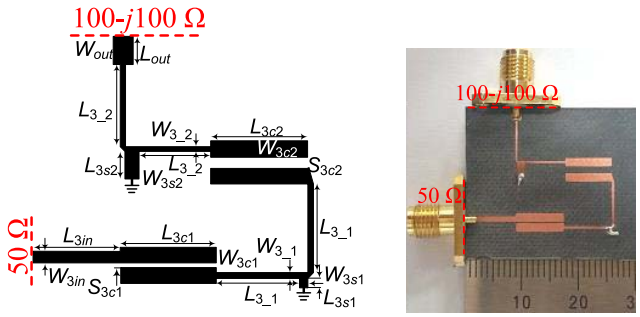

Fig. 16. Three-stage SIR BPF with the complex termination impedance. (a) Layout. (b) Photograph of fabricated circuit.

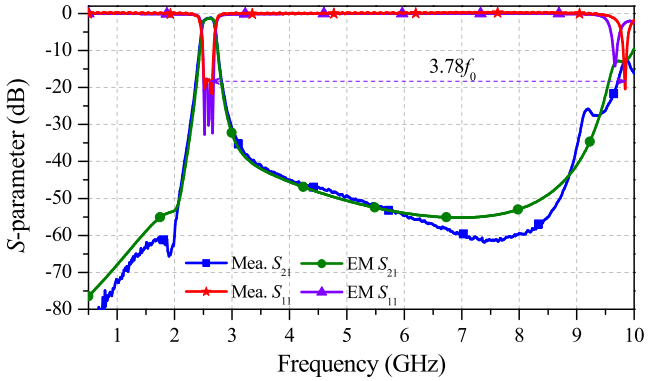

Fig. 17. Simulated and measured S-parameters of the three-stage SIR BPF with the complex impedance.

TABLE III
PHYSICAL DIMENSIONS OF THE THREE-STAGE SIR BPF WITH COMPLEX TERMINATION IMPEDANCE

$W_{3in}=0.88$	$S_{3c1}=0.35$	$W_{3S1}=0.55$	$W_{3\_2}=0.38$	$W_{3out}=1.78$
$L_{3in}=9$	$W_{3\_1}=0.38$	$W_{3c2}=1.45$	$L_{3\_2}=7.3$	$L_{3out}=2.5$
$W_{3c1}=1.4$	$L_{3\_1}=8$	$L_{3c2}=8.2$	$W_{3s2}=1.3$	
$L_{3c1}=8.4$	$L_{3S1}=0.2$	$S_{3c2}=1.25$	$L_{3s2}=2.47$	

$\phi_{34}=-6.09°$, $\theta_{34}=11.33°$, and $\theta_B=10.07°$. Fig. 16 shows the layout and a photograph of the fabricated filter. The EM simulation and measured S-parameter responses are shown in Fig. 17. The physical dimensions are shown in Table III. The overall circuit size of the fabricated BPF is 26.33 mm × 22.3 mm.

The measured insertion and return losses are 1.3 and 18.07 dB at $f_0 = 2.6$ GHz, respectively. Moreover, the passband insertion and return losses are better than 1.6 and 17.7 dB from 2.53 to 2.66 GHz (FBW = 5%), respectively. The lower- and upper-side stopband rejections of 30 dB are obtained from dc to 2.26 GHz and 2.97 to 9.1 GHz, respectively. The spurious frequency occurs at 9.83 GHz ($3.78f_0$). The transmission zero at the lower passband is occurred due to the coupling effect between a short-circuit stub and the input port. From this measurement, it has been proven that the proposed SIR BPF can be designed with the odd-order stages and complex termination impedance.

TABLE IV
COMPARISON RESULTS WITH RECENT EQUAL AND UNEQUAL TERMINATION IMPEDANCE BPFS

Ref.	f_0 (GHz)	Z_S-Z_L	Filter order	Controllable spurious	Resonator type	20 dB SB Atten. (GHz)	Design method
[5]	2	real-real	Even/odd	No	Microstrip	N.A	analytical
[6]	2.6	real-real	Even/odd	No	Microstrip	2.8 to 7	analytical
[7]	2.6	real-real	Even/odd	Yes	Microstrip	2.9 to 9	analytical
[8]	2.52	real-real	N.A	No	Microstrip	3.02 to 8.62	analytical
[10]	1	com-com	N.A	No	Microstrip	N.A	analytical
[15]	3.03	com-50	2	No	Cavity	N.A	analytical
[16]	2.5	com-50	Even/odd	No	Microstrip	N.A	optimizing
[24]	1.41	50-50	Even	Yes	Microstrip	1.6 to 7.5	analytical
This work	**2.6**	**com-com**	**Even/odd**	**Yes**	**Microstrip**	**2.8 to 9.8**	**analytical**

Abbreviation: com, complex; SB, stopband; atten, attenuation.

The merits of the proposed BPF are compared to those of previous publications in Table IV. The proposed work is more advantageous in terms of the complex terminations impedance, controllable spurious response, and the fact that it can be designed for either even or odd-order stages in the microstrip line.

IV. CONCLUSION

The new synthesis of complex termination impedances BPF was proposed and studied in this paper. The general design equations have been derived and validated with simulations using lossless TLs and coupled lines. The proposed filter can be simultaneously designed with arbitrary real and/or complex termination impedance and either even- or odd-order stages. In order to show the validity of the proposed filter, two complex terminations SIR BPFs were fabricated and measured. The simulated and measured results are consistent with the analysis. Since the complex termination impedance BPF presented in this paper can be designed with a narrowband, it is considered to be more reliable, more advantageous, and to have a low loss and more design flexibility. The proposed filter is expected to be co-designed with other microwave circuits for various applications in microwave circuit and system designs. Moreover, the concept idea of the proposed work might be applied to other kinds of the resonator such as the uniform impedance resonators and half-wavelength SIR. In the future work, wideband and/or dual-band BPFs with complex termination impedances are going to be studied.

REFERENCES

[1] D. M. Pozar, *Microwave Engineering*, 4th ed. New York, NY, USA: Wiley, 2012, pp. 48–87.

[2] P. Kim, G. Chaudhary, and Y. Jeong, "Enhancement impedance transforming ratios of coupled line impedance transformer with wide out-of-band suppression characteristics," *Microw. Opt. Technol. Lett.*, vol. 57, no. 7, pp. 1600–1603, Jul. 2015.

[3] P. Kim, J. Park, J. Jeong, S. Jeong, G. Chaudhary, and Y. Jeong, "High selectivity coupled line impedance transformer with second harmonic suppression," *J. Electromagn. Eng. Sci.*, vol. 16, no. 1, pp. 13–18, Jan. 2016.

[4] P. Kim, G. Chaudhary, and Y. Jeong, "Ultra-high transforming ratio coupled line impedance transformer with bandpass response," *IEEE Microw. Wireless Compon. Lett.*, vol. 25, no. 7, pp. 445–447, Jul. 2015.
[5] Q.-S. Wu and L. Zhu, "Short-ended coupled-line impedance transformers with ultrahigh transforming ratio and bandpass selectivity suitable for large load impedances," *IEEE Trans. Compon., Packag. Manuf. Technol.*, vol. 6, no. 5, pp. 767–774, May 2016.
[6] P. Kim, G. Chaudhary, and Y. Jeong, "Unequal termination impedance parallel-coupled lines band-pass filter with arbitrary image impedance," *J. Electromagn. Wave Appl.*, vol. 32, no. 8, pp. 984–996, 2018.
[7] P. Kim, G. Chaudhary, and Y. Jeong, "Impedance matching bandpass filter with a controllable spurious frequency based on $\lambda/2$ stepped impedance resonator," *IET Microw. Antennas Propag.*, vol. 12, no. 12, pp. 1993–2000, 2018. doi: 10.1049/iet-map.2018.5127.
[8] C.-W. Hsieh, S.-C. Lin, and J.-Y. Li, "Bandpass impedance transformers with extremely high transforming ratios using II-tapped feeds," *IEEE Access*, vol. 6, pp. 28193–28202, 2018.
[9] Y. Hsiao, C. Meng, and M. C. Li, "Analysis and design of broadband LC-ladder FET LNAs using noise match network," *IEEE Trans. Microw. Theory Techn.*, vol. 66, no. 2, pp. 987–1001, Feb. 2018.
[10] H. R. Ahn, "Complex impedance transformers consisting of only transmission-line sections," *IEEE Trans. Microw. Theory Techn.*, vol. 60, no. 7, pp. 2073–2084, Jul. 2012.
[11] X. Wang, M. Ohira, and Z. Ma, "A flexible two-section transmission-line transformer design approach for complex source and real load impedances," *IEICE Electron. Express*, vol. 14, no. 1, pp. 1–6, Dec. 2016.
[12] T. Jensen, V. Zhurbenko, V. Krozer, and P. Meincke, "Coupled transmission lines as impedance transformer," *IEEE Trans. Microw. Theory Techn.*, vol. 55, no. 12, pp. 2957–2965, Dec. 2007.
[13] R. Sinha and A. De, "Theory on matching network in viewpoint of transmission phase shift," *IEEE Trans. Microw. Theory Techn.*, vol. 64, no. 6, pp. 1704–1716, Jun. 2016.
[14] T. Zhang, W. Che, and H. Chen, "A wideband reconfigurable impedance matching network for complex loads," *IEEE Trans. Compon. Packag. Manuf. Technol.*, vol. 8, no. 6, pp. 1073–1081, Jun. 2018.
[15] K. Chen, J. Lee, W. J. Chappell, and D. Peroulis, "Co-design of highly efficient power amplifier and high-Q output bandpass filter," *IEEE Trans. Microw. Theory Techn.*, vol. 61, no. 11, pp. 3940–3950, Nov. 2013.
[16] X. Meng, C. Yu, Y. Liu, and Y. Wu, "Design approach for implementation of class-J broadband power amplifiers using synthesized band-pass and low-pass matching topology," *IEEE Trans. Microw. Theory Techn.*, vol. 65, no. 12, pp. 4984–4996, Dec. 2017.
[17] K. Chen and D. Peroulis, "Design of highly efficient broadband class-E power amplifier using synthesized low-pass matching networks," *IEEE Trans. Microw. Theory Techn.*, vol. 59, no. 12, pp. 3162–3173, Dec. 2011.
[18] J. Pang, S. He, Z. Dai, C. Huang, J. Peng, and F. You, "Design of continuous-mode GaN power amplifier with compact fundamental impedance solutions on package plane," *IET Microw., Antennas Propag.*, vol. 10, no. 10, pp. 1056–1064, Jul. 2016.
[19] J. Jeong, P. Kim, and Y. Jeong, "High efficiency power amplifier with frequency band selective matching networks," *Microw. Opt. Technol. Lett.*, vol. 57, no. 9, pp. 2031–2034, Sep. 2015.
[20] B. Zhang, G. Dong, Y. Wu, C. Yu, and Y. Liu, "Filtering push–pull power amplifier based on novel impedance transformers," *Electron. Lett.*, vol. 52, no. 17, pp. 1467–1469, Aug. 2016.
[21] X. Yu and S. Sun, "Computer aided design for dual-band filters with complex source and load impedances," *Int. J. RF Microw. Comput.-Aided Eng.*, vol. 28, no. 2, pp. 1–12, Sep. 2018.
[22] G. L. Matthaei, "Tables of Chebyshev impedance–transforming networks of low-pass filter form," *Proc. IEEE*, vol. 52, no. 8, pp. 939–963, Aug. 1964.
[23] S. Zhang and L. Zhu, "Synthesis method for even-order symmetrical chebyshev bandpass filters with alternative J/K inverters and $\lambda/4$ resonators," *IEEE Trans. Microw. Theory Techn.*, vol. 61, no. 2, pp. 808–816, Feb. 2013.
[24] K. U-Yen, E. J. Wollack, T. Doiron, J. Papapolymerou, and J. Laskar, "The design of a compact, wide spurious-free bandwidth bandpass filter using stepped impedance resonators," in *Proc. Eur. Microw. Conf.*, vol. 2, Apr. 2005, p. 4. doi: 10.1109/EUMC.2005.1610078.
[25] M. Makimoto and S. Yamashita, "Bandpass filters using parallel coupled stripline stepped impedance resonators," *IEEE Trans. Microw. Theory Techn.*, vol. 28, no. 12, pp. 1413–1417, Dec. 1980.
[26] S. Zhang, L. Zhu, and R. Weerasekera, "Synthesis of inline mixed coupled quasi-elliptic bandpass filters based on $\lambda/4$ resonators," *IEEE Trans. Microw. Theory Techn.*, vol. 63, no. 10, pp. 3487–3493, Oct. 2015.
[27] G. L. Matthaei, "Design of parallel-coupled resonator filters," *IEEE Microw. Mag.*, vol. 8, no. 5, pp. 78–87, Oct. 2007.
[28] S. Zhang, L. Zhu, and R. Li, "Compact quadruplet bandpass filter based on alternative J/K inverters and $\lambda/4$ resonators," *IEEE Microw. Wireless Compon. Lett.*, vol. 22, no. 5, pp. 224–226, May 2012.
[29] M. Makimoto and S. Yamashita, *Microwave Resonators and Filters for Wireless Communication*. Berlin, Germany: Springer-Verlag, 2001.

Phirun Kim (S'11–M'17) received the B.E. degree in electronics engineering from the National Polytechnic Institute of Cambodia (NPIC), Phnom Penh, Cambodia, in 2010, and the M.E. and Ph.D. degrees in electronics engineering from Chonbuk National University, Jeonju, South Korea, in 2013 and 2017, respectively.

He is currently a Contract Professor with the HOPE-IT Human Resource Development Center-BK21 PLUS, Division of Electronics Engineering, Chonbuk National University. He has authored or coauthored more than 40 papers in international journals and conference proceedings. His current research interests include planar passive filters, power dividers, impedance transformers, baluns, and high-efficiency power amplifiers.

Yongchae Jeong (M'99–SM'10) received the B.S.E.E., M.S.E.E., and Ph.D. degrees in electronics engineering from Sogang University, Seoul, South Korea, in 1989, 1991, and 1996, respectively.

From 1991 to 1998, he was a Senior Engineer with Samsung Electronics. In 1998, he joined the Division of Electronics Engineering, Chonbuk National University, Jeonju, South Korea. From 2006 to 2007, he was a Visiting Professor with the Georgia Institute of Technology, Atlanta, GA, USA. He is currently a Professor and a member of the Information Technology (IT) Convergence Research Center, and the Director of the HOPE-IT Human Resource Development Center, BK21 PLUS, Chonbuk National University. He has authored or coauthored more than 100 papers in international journals and conference proceedings. His current research interests include microwave passive and active circuits, mobile and satellite base-station RF systems, design of periodic defected transmission lines, and RF integrated circuit (RFIC) design.

Dr. Jeong is a member of the Korea Institute of Electromagnetic Engineering and Science (KIEES).